
DRIFT: DYNAMIC REGION-BASED INFERENCE FOR FAST OBJECT DETECTION ON MULTI-ACCELERATOR SOCS

ABSTRACT

Multi-object tracking (MOT) is a critical task in computer vision, involving detecting and tracking multiple objects over time and making informed decisions. State-of-the-art MOT systems rely on deep neural networks and transformer-based architectures for object detection, which can be computationally intensive and energy-consuming, especially in performance-limited and energy-efficient mobile computing environments. This paper addresses the challenge of improving MOT execution efficiency on heterogeneous system-on-chips (SoC) that integrate multiple accelerators, including GPUs, and domain-specific accelerators.

DRIFT leverages a novel multi-model, multi-accelerator execution strategy to improve latency and energy consumption without compromising critical operational accuracy. By identifying the locations of high-priority and low-priority objects in the frame, *DRIFT* can dynamically allocate computational resources to balance the detection of objects across multiple accelerators and sub-regions of the frame. This approach significantly reduces the size of input data and allows energy-efficient accelerators to be utilized. Evaluations using the MOT17 dataset demonstrate a reduction of up to 2.2x in latency, 3.8x in energy, and 2.2x in power draw, while preserving more than 95% of recall and 99% of detection accuracy, showcasing the effectiveness of *DRIFT* in real world scenarios.

1 INTRODUCTION

Multi-object tracking (MOT) is a principal computer vision task utilized in mobile and autonomous computing. It involves identifying and following multiple objects within a scene over time, which is essential to understand dynamic environments and making informed decisions. MOT systems typically consist of two main components: *detection*, which uses deep neural networks (DNNs) or detection-transformers (DETR) to identify objects in individual frames, and *tracking*, which associates these detections across frames to maintain consistent object identities (Wojke et al., 2017; Wojke & Bewley, 2018; Zhang et al.; Wang & Liao, 2024; Wang et al., 2024; Ge et al., 2021). In this work, we focus on real-time MOT on energy-efficient and performance-limited computing environments.

Many mobile and autonomous systems rely on multi-accelerator, *i.e.*, *heterogeneous*, system-on-chips (SoC) to efficiently execute various workloads such as MOT, rendering, video analytics and facial recognition (Dagli et al., 2022). In addition to CPUs and general purpose GPUs, these SoCs embed domain-specific processors such as deep learning accelerators (DLA) and programmable vision accelerators (PVA). Domain-specific accelerators are capable of running a specific set of functions in the domain much more efficiently, *i.e.*, less power spent for a unit of computation, making them highly favorable for energy- and power-constrained platforms. Figure 1 shows the breakdown of the total time spent processing a single frame with a MOT pipeline using a DNN-based object detector. The tracking algorithm is run on the CPU and accounts for only 14.5% of

the frame processing; whereas the object detection, although it runs on the much faster GPU, takes the remainder of the 26 ms execution time, while consuming around 95% of all the energy spent. An important realization is that mobile and autonomous systems usually have other GPU-based workloads, such as rendering, video encoding/decoding, video analytics, or facial recognition, which are often scheduled to run in parallel or in series with the MOT pipeline (Lee et al., 2021). As such, focusing on detection within a MOT pipeline has the greatest potential to improve power efficiency and reduce overall system latency.

In this paper, we explore the following question: *How could we improve MOT execution efficiency by reducing either the latency or energy spent per frame, without sacrificing critical requirements of operational accuracy?* In an attempt to find an answer, we come up with two important observations regarding MOT execution on multi-accelerator SoCs:

- (i) A comparison of inference time, power draw and energy consumption of the YOLOX (Ge et al., 2021) object detection (OD) model is shown in Figure 2. We run various parameter sizes of the model on the GPU and DLA of the popular NVIDIA Orin AGX mobile platform. Using DLA, the total energy spent on inference can be almost halved at the cost of a 1.42x increase in inference latency. Importantly, the GPU and DLA can be utilized concurrently to collaboratively parallelize DNN-based workloads. *Current MOT approaches do not consider collaborative execution, because the execution pipeline is not parallel.* Using multiple accelerators would provide performance and energy benefits if there were a method to parallelize the MOT pipeline.

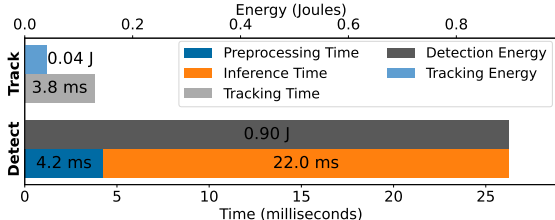


Figure 1: Comparison of the runtimes of YOLOv10 (Wang et al., 2024) M with 1280x1280 input size and ByteTrack (Zhang et al.) on an Orin AGX 64GB using an off-the-shelf single-threaded implementation.

(ii) While the state-of-the-art practice is to feed the entire camera input to the detection model, the portion of the input image that is large enough to perform accurate OD may be much smaller than the entire input. Moreover, *not all tracked objects may be of critical importance*. Figure 3 depicts the smallest region that contains bounding boxes of the most important objects in red, e.g., cars or pedestrians, for a variety of videos in the MOT17 dataset (Milan et al., 2016). Additionally, the regions containing objects of lesser importance, shown in blue, indicate situations where detection results matter less, such as when objects are stationary or far from the path of travel. In particular, the region of interest (ROI) (Chen et al., 2021) shown in green, which typically contains all objects, is significantly larger than the combination of the red and blue regions.

By separating each frame into multiple regions, we can distribute the detection for a single frame across several accelerators, enabling parallel execution and potentially improving the overall efficiency of the system. This strategy is based on three key observations: objects within a frame are often clustered; the clusters tend to cover only a fraction of the full image; and the spatial distribution of objects can change rapidly as new objects enter or leave the scene. However, several challenges arise with this approach.

- C1:** Determining how to efficiently divide frames into regions while minimizing computational overhead.
- C2:** Identifying when new objects appear outside the established regions.
- C3:** Estimating current DNN accuracy based only on the limited available context.
- C4:** Managing multi and concurrent model execution across multiple accelerators without additional overhead.

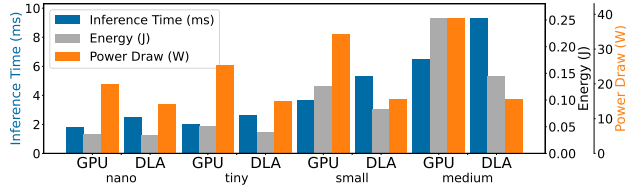


Figure 2: Comparison of GPU vs. DLA inference metrics on NVIDIA Orin AGX 64GB. Each version of YOLOX (nano, tiny, small, medium) uses the default input size as defined by the maintainers being 416, 416, 640, and 640 respectively.



Figure 3: MOT17 scenarios and corresponding example regions of high priority (red), low priority (blue), and overall region-of-interests (green) detection regions.

To address these challenges we propose a new approach to improve the efficiency of MOT execution.

We introduce *DRIFT*¹, a Dynamic Region-based Inference for Fast Object DeTection. We devise a novel, multi-model, multi-accelerator execution methodology that significantly improves the latency and energy consumption of OD in MOT pipelines. *DRIFT* achieves this by treating user-defined high-priority (HP) and low-priority (LP) classes of objects separately. During runtime, we process the region of the frame containing all HP objects using the original detection model (or an equivalent) on a reduced input to improve latency. For the remainder of the frame, we employ faster and/or lower-accuracy models, which can run in parallel on another accelerator. The detection accuracy for LP objects is lower-bounded by a user specified knob. *DRIFT* is versatile and could work with various types of object detection models including DNNs and DETRs.

The contributions of our work are as follows:

- We propose a novel MOT approach that improves latency, energy-consumption, and power-draw in mobile platforms by reducing the size of the input data without sacrificing the detection accuracy for high-priority objects.
- We efficiently split captured frames into high- and low-priority regions according to a set of user-defined classes.
- We utilize energy-efficient accelerators to detect low-priority objects collaboratively while meeting a user-determined detection accuracy threshold.
- We present a unique methodology for merging the output of multiple object detection models and derive the current context and assessment of the model performance.
- We integrate a very-low-overhead scheduler capable of handling the large state-space of possible model selections and accelerator mappings.
- We evaluate the efficiency of our approach on the industry-standard MOT17 dataset and show a reduction of up to **2.2x** in latency, **3.8x** in energy, and **2.2x** in power draw, while operating at a higher recall and detection accuracy than 95% and 99%, respectively.

2 RELATED WORK

Multi-object tracking (MOT): State-of-the-art MOT solutions often utilize a two-stage detection process

¹*DRIFT* source code will be released upon publication.

followed by tracking, with a single-pass DNN using a GPU as the primary detector. The tracking portion can either consist of traditional CPU-based implementations to label individual detections with unique IDs (Liang et al., 2022; Pang et al., 2021) or include additional DNN inferences to improve tracking accuracy (Ravindran et al., 2020; Zhang et al.; Du et al., 2023). All such MOT works do not consider the role of dynamically allocating detection resources and how they can be augmented, instead treating the detection stage as unchangeable during runtime. *DRIFT instead focuses on improving detection latency while utilizing existing tracking algorithms.*

Scheduling for latency, energy, and accuracy: Scheduling DNN workloads to improve latency, energy efficiency, or accuracy has been an open research area for more than a decade. BigLittle (Park et al., 2015) proposes switching back and forth between a large and a small classifier to save energy and minimize latency while processing a set of frames. NestDNN (Fang et al., 2018) focuses on splitting a single DNN model into multiple subgraphs and pruning such graphs to balance accuracy, latency, and energy trade-offs. Hax-CoNN (Dagli & Belviranli, 2024) focuses on fine-grained optimizations, CARin (Panopoulos et al., 2024) targets multi-application level objectives. *DRIFT, instead of focusing on improving concurrent execution or latency through advanced low-level methodologies, demonstrates that system-level scheduling, scalable input sizes, and input partitioning are sufficient to manage multi-DNN inference schemes while accounting for additional computational requirements in real-world scenarios.*

Context-aware Inference: Only a small set of studies offer context-aware approaches to enhance the use of DNN models. CACTUS (Rastikerdar et al., 2024) splits the classification into many smaller problems by creating a set of micro-classifiers, where each classifier handles a subset of classes. The inference time is minimized by identifying the context of the current image and performing only a few micro-classifications. However, this method introduces high complexity during context changes and requires custom training schemes. SHIFT (Davis & Belviranli, 2024) focuses on switching between different models at runtime based on the confidence score output, as well as the differences between frames and detected bounding boxes. *DRIFT reduces runtime latency by scaling the input size based on the spatial context of object detections and can consider more than a single-class / single-object scenario during context identification.*

Region-of-Interest for Object Detection: Methodologies using a system-level region-of-interest (ROI) to constrain OD typically rely on manual or domain-specific automated computer vision algorithms. These approaches, such as Flex-Patch (Yang et al.) and others (Jiang et al., 2021; Gokarn

Related Work \ Feature	HaxCoNN	CARin	BigLittle	NestDNN	CACTUS	SHIFT	FlexPatch	<i>DRIFT</i>
Context Aware	✗	✗	✓	✗	✓	✓	✓	✓
Accuracy Predictions	✗	✗	✗	✗	✗	✗	✗	✓
Concurrent DNNs	✓	✓	✗	✗	✗	✗	✗	✓
Non-GPU Accelerators	✓	✓	✗	✗	✗	✓	✗	✓
Object Detection	✗	✗	✗	✗	✗	✓	✓	✓
No Additional Training	✓	✓	✓	✗	✗	✓	✓	✓
ROI Focusing	✗	✗	✗	✗	✗	✗	✓	✓
Low Overhead	✓	✗	✗	✓	✗	✓	✗	✓

Table 1: Comparison of the features offered by related works.

et al., 2023; Dhonde et al., 2023; Girshick et al., 2014; Girshick, 2015; Ren et al., 2016), either rely on computationally expensive algorithms to determine candidate regions, embed significant initialization overhead, necessitate continuous calibration, or run additional DNN inference to determine ROIs. *DRIFT utilizes a generic automatic ROI-finding method that does not require additional computation, operates solely on existing OD outputs, and does not require additional runtime input, unlike previous methods.*

Table 1 provides an overview of the features offered by the most relevant works and *DRIFT*: (i) the capability to detect contextual information embedded in the input data stream, (ii) the ability to predict accuracy as a metric in their methodology, (iii) concurrent execution of DNNs, (iv) utilization of domain-specific accelerators, (v) targeting object detection workloads, (vi) no requirement for additional training, pruning, or fine-tuning to achieve performance, (vii) the ability to target specific data within an input stream by utilizing ROIs, and (viii) a focus on low runtime overhead for computation without offloading. *Safe and efficient operation of MOT pipelines with an optimized detection stage requires a holistic consideration of all these features. To the best of our knowledge, only DRIFT achieves this goal.*

3 PROPOSED APPROACH: *DRIFT*

DRIFT relies on four main components to enable a priority-based MOT scheme and save latency, power, and energy without losing accuracy on the HP objects: (i) *High and low priority splitting algorithm* which enables *DRIFT* to split a single frame into parallel regions with varying accuracy goals, (ii) *the frame packing algorithm* which enables low priority objects to be represented with less data, (iii) *accuracy and latency models* to predict which model to use for LP and HP detection, and (iv) *the runtime scheduler* which dynamically maps models to accelerators (*i.e.*, GPU and DLA) so that the accuracy constraints are met while minimizing overall runtime, *i.e.*, frame latency. An overview of the data flow and components is given in Figure 4.

3.1 Identification of High Priority Regions

High priority regions are determined based on a set of user defined priority class labels. For a set of detections on the entire image, the detections with class labels in the priority set are isolated. Then, the bounding box encasing all

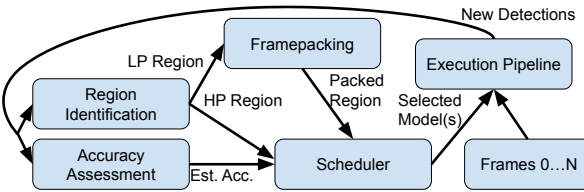


Figure 4: Overview of the *DRIFT* setup and how each component connects. Region identification, framepacking, accuracy/latency modeling, and scheduling are outlined in Section 3.1, Section 3.2, Section 3.3, and Section 3.4 respectively.

isolated detections is generated. This new bounding box is used as the *HP region* for the next frame. The remainder of the frame is the LP region and is processed further by the frame packing algorithm described next in Section 3.2. Since MOT is designed for continuous frame sequences, there is an implicit assumption that objects will not significantly change position frame-to-frame. This assumption is used in MOT algorithms such as SORT, DeepSORT, and ByteTrack (Wojke et al., 2017; Wojke & Bewley, 2018; Zhang et al.). Thus, when an HP region is identified in the current frame, it will still be present in the next frame. A small amount of padding is added to account for object movement between frames to ensure objects do not get cut off. This is a standard practice for methodologies that utilize regions of interest (ROIs) in an OD context (Yang et al.; Dhonde et al., 2023). By assessing the priority based on a set of user-defined class labels, the relevant HP region can be determined with almost no overhead and requires only a single iteration over the set of detections, addressing challenge C1.

It is possible that the LP region will contain objects of the HP class in one of these conditions: 1) the HP/LP model cannot detect the object, 2) the HP model loses detection of the object and the object moves to LP region, 3) the movement of camera results in new objects appearing in the frames, and 4) objects move into the scene when camera is static. In such cases, the LP model will detect objects with HP classes, and the HP area will be redefined to include them.

All objects in the HP region, regardless of their class, will be detected by the HP model. Therefore, corresponding pixels in the HP region should be excluded from the LP model’s inputs to save computational resources. A naive solution to this problem is to black out the HP region and then perform inference on the remaining regions. By this way, duplicate detections do not need to be filtered on the CPU side post inference, providing a potential optimization. However, this method wastes computation since the LP model will still process the blacked-out region. A more efficient solution is to create a new image for the LP region which has been reorganized to completely exclude the HP region. This method would have three benefits; i) there will be no wasted computation where regions of the image get processed by

multiple DNNs; ii) the data size will be smaller, allowing for a smaller input size or less sub-sampling during inference; and iii) we will be able to use the DLA to parallelize computation and save energy.

Based on the insights detailed above, we introduce a novel frame packing algorithm to efficiently process LP regions.

3.2 Frame Packing for Low Priority Regions

Our frame packing algorithm is based on simulated annealing and 2D bin packing: First, regions that are not likely to contain detectable objects are removed, reducing the overall data size. Then, regions are bin-packed into a new image, minimizing the difference between the height and width, which in turn minimizes distortion and resolution loss during preprocessing for the OD DNN.

Formulation: To reduce the computational complexity of determining the importance of regions of the input stream, a predetermined grid is maintained, where each cell maps to a fixed square region of the frame. Each grid cell tracks the number of detections within itself. Once detections are generated for a frame, each cell of the grid has its counter incremented by the number of objects that intersect that cell. All cells that did not have any intersecting detections have their counter decremented. Using this simple counting methodology, the relevance of each cell can be determined. The simulated annealing algorithm assigns a probability to include the cell using the current frame number and the detection counter. The probability is defined in Equation 1,

$$P_{exp} = \min \left\{ 1, \max \left\{ p_{min}, e^{-\alpha c} + \min \left\{ 1, \frac{d}{\min\{FPS, c+1\}} \right\} \right\} \right\} \quad (1)$$

where c is the global frame counter, d is current detection counter for the cell, α is the cooling rate, FPS is the frame rate of the sequence, and p_{min} is the minimum probability. The detection tracking counter and the frames captured since initialization provide enough contextual information to accurately identify regions that can be excluded from the LP model inference. Importantly, it is possible that no cells are selected by simulated annealing, meaning that no additional inference pass is required for that frame and only the HP region gets processed. Intuitively, for every region, its probability to be sampled will increase if more than 1 object is present, remain the same with 1 object present, and decrease to p_{min} if no objects are present.

Once a set of grid cells has been generated by simulated annealing, the corresponding image regions represented by these cells are packed into a new image. Since the cells are on a structured grid pattern, some of the cells can be grouped together to form connected components. By forming groups of cells, more spatial contextual information can be preserved. This prevents objects that span multiple cells from being split into smaller pieces and not being detected. To make re-packing of the groups easier, only connected component groups which are dense, *i.e.*, are fully filled

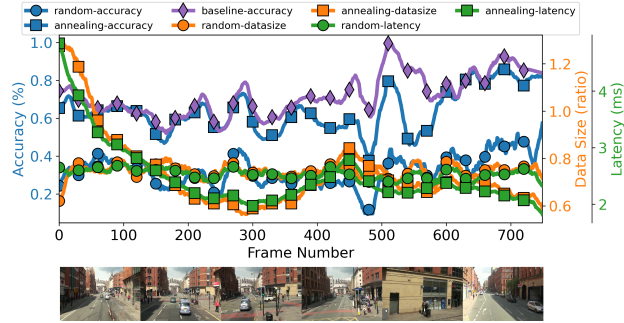


Figure 5: Analysis of frame packing reduction ratio, latency, and the maximum recoverable accuracy using the baseline YOLOv10 M 1280x1280 DNN on the MOT17-13 sequence.

rectangles, are considered. Since groups of cells will have many different shapes, forming a new image from these groups is NP-Complete since it can be represented as 2D bin packing problem (Korte & Vygen, 2007). As such, we use the shelf-based 2D bin packing heuristic algorithm with a minor modification to attempt to pack the regions into a square input is important, as the standard configurations of object detection models such as YOLO are trained on square images.

Algorithm: The procedure for the bin-packing algorithm is presented in Algorithm 2 in Appendix A.2. The input image I is the current frame from the sequence and the groups G is the set of all connected component groups or standalone cells. The algorithm works as follows: (Lines 1-3): If there are no groups, return an empty image. (4): Sort the groups by descending size to pack the largest groups first. (5): Define the target size of the ideal square image. (6): Define the set of shelves. (7-16): For all groups, attempt to greedily place the group on the first shelf with the same width and available height, otherwise create a new shelf. (17-19): Create the new image based on the shelf sizes. (20-31): Iterate over each shelf, then iterate over each cell –all exist since width matching and dense groups were required–, and copy each cell from I into P to fill in the new image.

Once the new LP region image is formed, it is passed to the LP model for detection. To convert detections from the packed LP image back to the real frame coordinates, the bin-packing algorithm saves a 2D set of offsets. Then, each bounding box is converted to cell coordinates in the packed image. These cell coordinates are used to get the offset to transform the bounding box to the original frame.

Verification: In order to verify that the frame packing methodology is able to keep the relevant regions of the image within the packed representation, we evaluate its recall against the baseline model defined in Section 4. The experiment is set up as follows: 1) the entire frame is given as the input frame to be packed instead of just a subset; 2) the detections used to update the grid are the detections of the baseline model on the entire frame; and 3) the recall of the baseline model on the packed image is the displayed ac-

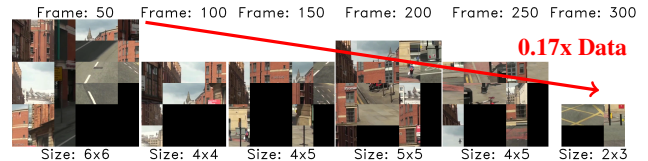


Figure 6: Comparison of the packed grid cells after blocks of frames have been processed via simulated annealing. Detection results are from the baseline YOLOv10 M 1280x1280 DNN running on the entire image.

curacy. As can be observed in Figure 5, the baseline model can recover most of the detections while removing up to 40% of the image. The minimum probability of the annealing function was set to 10% with the grid size to be equal to one tenth of the larger dimension of the images. A random sampling method was also created that will sample 75% of the image to be packed. Both methods utilize the bin packing methodology to create the new packed image. As can be observed, the random methodology does not recover the same accuracy as the annealing based methodology, showcasing sampling cells with simulated annealing can adapt to the scenario sufficiently after a small warm-up period. A visual example of the frame-packing process is presented in Figure 6. As shown, within 300 frames (or 10 seconds), the simulated annealing and bin-packing algorithms work together to reduce the LP data to be processed to just 7% of the overall image resolution (10% when accounting for inefficiently packed space). Having such small input sizes significantly increases the optimization capability of a parallel inference for LP. Using fast heuristics to create the LP region for detection, DRIFT is able to effectively solve challenge C2.

3.3 Predicting Model Accuracy and Latency

To effectively schedule object detection DNNs at runtime, an estimation of their accuracy and latency needs to be modeled beforehand so that quick scheduling decisions could be made. Ideally, such a model should be built using ground truths for the best representation of accuracy. However, ground truth data will not be available for the frames encountered during runtime, and the closest metric reported by the DNN execution is the confidence scores, which do not directly represent the accuracy of the model. To quantify accuracy, we use the F1 score, the geometric mean between precision and recall, as the accuracy metric (Smith et al., 2005). The higher the F1 score, the more precise the model and the more objects the model can recall. During runtime, the only metric available to quantify accuracy is the confidence score. However, since the confidence score primarily reflects the certainty of positive detections, it is an incomplete metric. Consider the case where a model generates high confidence values but misses many objects. In this scenario, the recall will suffer significantly, but the precision of the model remains high. This creates a non-linear relationship which will not be accurately predicted at runtime. Thus, the F1 score is used to model the hidden relationship

275 between confidence score, precision, and recall.

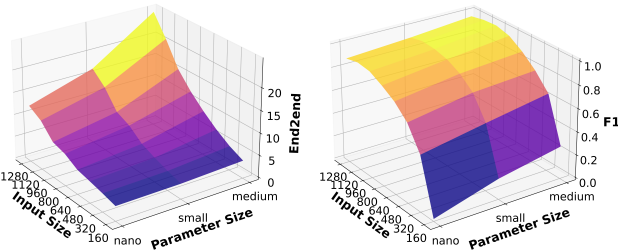
276 In order to generate runtime F1 score estimates, we develop
 277 a 2D setup of linear estimators. For each model, an estimator
 278 is trained to predict the F1 score of itself and every other
 279 model based on the mean confidence value of the set of
 280 detections on a given frame. To train the estimators, we use
 281 the validation set of the dataset on which the object detection
 282 DNN was trained. Importantly, the difficulty of the datasets
 283 may be different, *i.e.*, the F1 score distribution can change
 284 depending on whether the DNN is running on COCO17 (Lin
 285 et al., 2015) images (with which YOLO was trained) or
 286 MOT17 frames (which we use in our experiments). To
 287 account for this, a scaling factor is calculated based on
 288 the median F1 score that will be used along with the user-
 289 defined knobs in the runtime scheduler.
 290

291 A visualization of the characterizations for end-to-end in-
 292 ference time and the F1 score can be found in Figure 7.
 293 As expected, increasing computational resources results in
 294 higher F1 scores. We observe that reductions in parameter
 295 sizes can be offset by proportionally increasing input sizes,
 296 effectively recovering performance. These relationships are
 297 captured by the 2D linear estimator setup, enabling dynamic
 298 runtime adjustments to balance input and parameter sizes.
 299 Using a lightweight set of linear estimators trained to predict
 300 the F1 score of all models from the confidence score of a
 301 single model, DRIFT is able to predict accuracy without
 302 adding significant latency, hence solving challenge C3.

3.4 Runtime Scheduler

303 The runtime scheduler determines which models to execute
 304 for the HP and LP regions. HP regions are always executed
 305 on the GPU, as they are the critical execution path. Based
 306 on the estimated latency, the scheduler decides whether to
 307 execute an LP region on the DLA (in parallel) or on the
 308 GPU (in series), while maintaining a user defined accuracy
 309 threshold for the LP region. The scheduler accomplishes
 310 this using a combination of offline and online approaches.
 311

312 *Offline:* We characterize all possible GPU(HP)+GPU(LP)
 313 and GPU(HP)+DLA(LP) combinations based on the set
 314 of all available OD models. Schedules will be evaluated
 315 based on runtime characteristics including pre-processing,
 316 inference, post-processing, and end-to-end latency.
 317



318
 319
 320
 321
 322
 323
 324
 325
 326
 327
 328
 329
 330
 331
 332
 333
 334
 335
 336
 337
 338
 339
 340
 341
 342
 343
 344
 345
 346
 347
 348
 349
 350
 351
 352
 353
 354
 355
 356
 357
 358
 359
 360
 361
 362
 363
 364
 365
 366
 367
 368
 369
 370
 371
 372
 373
 374
 375
 376
 377
 378
 379
 380
 381
 382
 383
 384
 385
 386
 387
 388
 389
 390
 391
 392
 393
 394
 395
 396
 397
 398
 399
 400
 401
 402
 403
 404
 405
 406
 407
 408
 409
 410
 411
 412
 413
 414
 415
 416
 417
 418
 419
 420
 421
 422
 423
 424
 425
 426
 427
 428
 429
 430
 431
 432
 433
 434
 435
 436
 437
 438
 439
 440
 441
 442
 443
 444
 445
 446
 447
 448
 449
 450
 451
 452
 453
 454
 455
 456
 457
 458
 459
 460
 461
 462
 463
 464
 465
 466
 467
 468
 469
 470
 471
 472
 473
 474
 475
 476
 477
 478
 479
 480
 481
 482
 483
 484
 485
 486
 487
 488
 489
 490
 491
 492
 493
 494
 495
 496
 497
 498
 499
 500
 501
 502
 503
 504
 505
 506
 507
 508
 509
 510
 511
 512
 513
 514
 515
 516
 517
 518
 519
 520
 521
 522
 523
 524
 525
 526
 527
 528
 529
 530
 531
 532
 533
 534
 535
 536
 537
 538
 539
 540
 541
 542
 543
 544
 545
 546
 547
 548
 549
 550
 551
 552
 553
 554
 555
 556
 557
 558
 559
 560
 561
 562
 563
 564
 565
 566
 567
 568
 569
 570
 571
 572
 573
 574
 575
 576
 577
 578
 579
 580
 581
 582
 583
 584
 585
 586
 587
 588
 589
 590
 591
 592
 593
 594
 595
 596
 597
 598
 599
 600
 601
 602
 603
 604
 605
 606
 607
 608
 609
 610
 611
 612
 613
 614
 615
 616
 617
 618
 619
 620
 621
 622
 623
 624
 625
 626
 627
 628
 629
 630
 631
 632
 633
 634
 635
 636
 637
 638
 639
 640
 641
 642
 643
 644
 645
 646
 647
 648
 649
 650
 651
 652
 653
 654
 655
 656
 657
 658
 659
 660
 661
 662
 663
 664
 665
 666
 667
 668
 669
 670
 671
 672
 673
 674
 675
 676
 677
 678
 679
 680
 681
 682
 683
 684
 685
 686
 687
 688
 689
 690
 691
 692
 693
 694
 695
 696
 697
 698
 699
 700
 701
 702
 703
 704
 705
 706
 707
 708
 709
 710
 711
 712
 713
 714
 715
 716
 717
 718
 719
 720
 721
 722
 723
 724
 725
 726
 727
 728
 729
 730
 731
 732
 733
 734
 735
 736
 737
 738
 739
 740
 741
 742
 743
 744
 745
 746
 747
 748
 749
 750
 751
 752
 753
 754
 755
 756
 757
 758
 759
 760
 761
 762
 763
 764
 765
 766
 767
 768
 769
 770
 771
 772
 773
 774
 775
 776
 777
 778
 779
 780
 781
 782
 783
 784
 785
 786
 787
 788
 789
 790
 791
 792
 793
 794
 795
 796
 797
 798
 799
 800
 801
 802
 803
 804
 805
 806
 807
 808
 809
 810
 811
 812
 813
 814
 815
 816
 817
 818
 819
 820
 821
 822
 823
 824
 825
 826
 827
 828
 829
 830
 831
 832
 833
 834
 835
 836
 837
 838
 839
 840
 841
 842
 843
 844
 845
 846
 847
 848
 849
 850
 851
 852
 853
 854
 855
 856
 857
 858
 859
 860
 861
 862
 863
 864
 865
 866
 867
 868
 869
 870
 871
 872
 873
 874
 875
 876
 877
 878
 879
 880
 881
 882
 883
 884
 885
 886
 887
 888
 889
 890
 891
 892
 893
 894
 895
 896
 897
 898
 899
 900
 901
 902
 903
 904
 905
 906
 907
 908
 909
 910
 911
 912
 913
 914
 915
 916
 917
 918
 919
 920
 921
 922
 923
 924
 925
 926
 927
 928
 929
 930
 931
 932
 933
 934
 935
 936
 937
 938
 939
 940
 941
 942
 943
 944
 945
 946
 947
 948
 949
 950
 951
 952
 953
 954
 955
 956
 957
 958
 959
 960
 961
 962
 963
 964
 965
 966
 967
 968
 969
 970
 971
 972
 973
 974
 975
 976
 977
 978
 979
 980
 981
 982
 983
 984
 985
 986
 987
 988
 989
 990
 991
 992
 993
 994
 995
 996
 997
 998
 999
 1000
 1001
 1002
 1003
 1004
 1005
 1006
 1007
 1008
 1009
 1010
 1011
 1012
 1013
 1014
 1015
 1016
 1017
 1018
 1019
 1020
 1021
 1022
 1023
 1024
 1025
 1026
 1027
 1028
 1029
 1030
 1031
 1032
 1033
 1034
 1035
 1036
 1037
 1038
 1039
 1040
 1041
 1042
 1043
 1044
 1045
 1046
 1047
 1048
 1049
 1050
 1051
 1052
 1053
 1054
 1055
 1056
 1057
 1058
 1059
 1060
 1061
 1062
 1063
 1064
 1065
 1066
 1067
 1068
 1069
 1070
 1071
 1072
 1073
 1074
 1075
 1076
 1077
 1078
 1079
 1080
 1081
 1082
 1083
 1084
 1085
 1086
 1087
 1088
 1089
 1090
 1091
 1092
 1093
 1094
 1095
 1096
 1097
 1098
 1099
 1100
 1101
 1102
 1103
 1104
 1105
 1106
 1107
 1108
 1109
 1110
 1111
 1112
 1113
 1114
 1115
 1116
 1117
 1118
 1119
 1120
 1121
 1122
 1123
 1124
 1125
 1126
 1127
 1128
 1129
 1130
 1131
 1132
 1133
 1134
 1135
 1136
 1137
 1138
 1139
 1140
 1141
 1142
 1143
 1144
 1145
 1146
 1147
 1148
 1149
 1150
 1151
 1152
 1153
 1154
 1155
 1156
 1157
 1158
 1159
 1160
 1161
 1162
 1163
 1164
 1165
 1166
 1167
 1168
 1169
 1170
 1171
 1172
 1173
 1174
 1175
 1176
 1177
 1178
 1179
 1180
 1181
 1182
 1183
 1184
 1185
 1186
 1187
 1188
 1189
 1190
 1191
 1192
 1193
 1194
 1195
 1196
 1197
 1198
 1199
 1200
 1201
 1202
 1203
 1204
 1205
 1206
 1207
 1208
 1209
 1210
 1211
 1212
 1213
 1214
 1215
 1216
 1217
 1218
 1219
 1220
 1221
 1222
 1223
 1224
 1225
 1226
 1227
 1228
 1229
 1230
 1231
 1232
 1233
 1234
 1235
 1236
 1237
 1238
 1239
 1240
 1241
 1242
 1243
 1244
 1245
 1246
 1247
 1248
 1249
 1250
 1251
 1252
 1253
 1254
 1255
 1256
 1257
 1258
 1259
 1260
 1261
 1262
 1263
 1264
 1265
 1266
 1267
 1268
 1269
 1270
 1271
 1272
 1273
 1274
 1275
 1276
 1277
 1278
 1279
 1280
 1281
 1282
 1283
 1284
 1285
 1286
 1287
 1288
 1289
 1290
 1291
 1292
 1293
 1294
 1295
 1296
 1297
 1298
 1299
 1300
 1301
 1302
 1303
 1304
 1305
 1306
 1307
 1308
 1309
 1310
 1311
 1312
 1313
 1314
 1315
 1316
 1317
 1318
 1319
 1320
 1321
 1322
 1323
 1324
 1325
 1326
 1327
 1328
 1329
 1330
 1331
 1332
 1333
 1334
 1335
 1336
 1337
 1338
 1339
 1340
 1341
 1342
 1343
 1344
 1345
 1346
 1347
 1348
 1349
 1350
 1351
 1352
 1353
 1354
 1355
 1356
 1357
 1358
 1359
 1360
 1361
 1362
 1363
 1364
 1365
 1366
 1367
 1368
 1369
 1370
 1371
 1372
 1373
 1374
 1375
 1376
 1377
 1378
 1379
 1380
 1381
 1382
 1383
 1384
 1385
 1386
 1387
 1388
 1389
 1390
 1391
 1392
 1393
 1394
 1395
 1396
 1397
 1398
 1399
 1400
 1401
 1402
 1403
 1404
 1405
 1406
 1407
 1408
 1409
 1410
 1411
 1412
 1413
 1414
 1415
 1416
 1417
 1418
 1419
 1420
 1421
 1422
 1423
 1424
 1425
 1426
 1427
 1428
 1429
 1430
 1431
 1432
 1433
 1434
 1435
 1436
 1437
 1438
 1439
 1440
 1441
 1442
 1443
 1444
 1445
 1446
 1447
 1448
 1449
 1450
 1451
 1452
 1453
 1454
 1455
 1456
 1457
 1458
 1459
 1460
 1461
 1462
 1463
 1464
 1465
 1466
 1467
 1468
 1469
 1470
 1471
 1472
 1473
 1474
 1475
 1476
 1477
 1478
 1479
 1480
 1481
 1482
 1483
 1484
 1485
 1486
 1487
 1488
 1489
 1490
 1491
 1492
 1493
 1494
 1495
 1496
 1497
 1498
 1499
 1500
 1501
 1502
 1503
 1504
 1505
 1506
 1507
 1508
 1509
 1510
 1511
 1512
 1513
 1514
 1515
 1516
 1517
 1518
 1519
 1520
 1521
 1522
 1523
 1524
 1525
 1526
 1527
 1528
 1529
 1530
 1531
 1532
 1533
 1534
 1535
 1536
 1537
 1538
 1539
 1540
 1541
 1542
 1543
 1544
 1545
 1546
 1547
 1548
 1549
 1550
 1551
 1552
 1553
 1554
 1555
 1556
 1557
 1558
 1559
 1560
 1561
 1562
 1563
 1564
 1565
 1566
 1567
 1568
 1569
 1570
 1571
 1572
 1573
 1574
 1575
 1576
 1577
 1578
 1579
 1580
 1581
 1582
 1583
 1584
 1585
 1586
 1587
 1588
 1589
 1590
 1591
 1592
 1593
 1594
 1595
 1596
 1597
 1598
 1599
 1600
 1601
 1602
 1603
 1604
 1605
 1606
 1607
 1608
 1609
 1610
 1611
 1612
 1613
 1614
 1615
 1616
 1617
 1618
 1619
 1620
 1621
 1622
 1623
 1624
 1625
 1626
 1627
 1628
 1629
 1630
 1631
 1632
 1633
 1634
 1635
 1636
 1637
 1638
 1639
 1640
 1641
 1642
 1643
 1644
 1645
 1646
 1647
 1648
 1649
 1650
 1651
 1652
 1653
 1654
 1655
 1656
 1657
 1658
 1659
 1660
 1661
 1662
 1663
 1664
 1665
 1666
 1667
 1668
 1669
 1670
 1671
 1672
 1673
 1674
 1675
 1676
 1677
 1678
 1679
 1

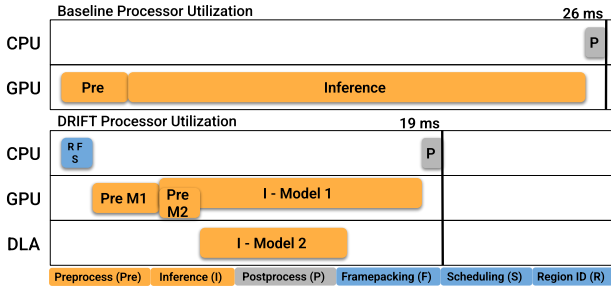


Figure 8: Overview of the processor utilization of the baseline OD DNN pipeline and the proposed *DRIFT* computational pipeline. Computational blocks with a hardware acceleration requirement are shown in orange, CPU-based computation is shown in grey, and additional computational for *DRIFT* is shown in blue.

edge cases where objects are large relative to total image size. (18-22): If there are models that can run the HP region with scaling down more than baseline, use the fastest one, otherwise use the most accurate of all models. (23): Enumerate possible schedules using the model determined for the HP region. (24-25): Predict current F1 scores based on previous detections, *i.e.*, recalls, from the LP models, (26-32): Filter out the schedules having an LP model that does not meet the accuracy threshold. (33-38): If there are schedules which meet the LP accuracy threshold, use the fastest one, otherwise use the most accurate schedule.

Once a desired schedule is found, the corresponding detection algorithms are executed on designated accelerators. The locations of the detected objects are then fed into the ByteTrack tracking algorithm. Please note that the scheduler falls back to the baseline YOLO model for the entire frame if it realizes that the HP-LP approach would not provide latency benefits. By avoiding fine-grained optimizations and using heuristics tuned to the MOT problem, *DRIFT* is able to effectively consider concurrent schedules and model swaps at runtime with low overhead, solving challenge C4.

3.5 Summary

Figure 8 shows an example of how the proposed *DRIFT* OD pipeline redistributes the computational load across available hardware resources. While the baseline approach processes the entire frame with a single large pass, our approach leverages multiple accelerators (GPU for HP and DLA for LP). The example illustrates that, even though additional computation is introduced for region identification, frame packing, and scheduling, the additional overhead is far less than the saved latency, resulting in a lower overall latency. *By splitting frames into multiple detection passes, the utilization of the system can be improved, allowing for lower latency and energy usage due to the use of DLAs.*

4 EXPERIMENTAL SETUP

Hardware: We evaluate *DRIFT* on an NVIDIA Orin AGX 64GB development kit (Orin), a popular multi-accelerator platform used in mobile, edge, and autonomous computing.

The Orin is equipped with 8 Arm Cortex-A78AE CPU cores, an Ampere generation GPU, a pair of second-generation NVIDIA DLA cores, and 64GB of LPDDR5 shared memory. We utilize only a single DLA core at a time, due to the restrictions deployed by the vendor runtime.

Object detection models: In our implementation, we use parameterizations of the DNN-based YOLOv10 and YOLO-X models, and detection transformer-based RF-DETR models. We utilize YOLOv10 on the GPU due to its low inference time and its elimination of the need for non-max-suppression (NMS). The YOLOv10 *nano*, *small*, and *medium* models quantized to fp16, are used with possible input sizes between 160 and 1280 with increments of 160, resulting in 24 possible combinations. For execution on the DLA, we used YOLOX models instead since v10 cannot run on DLAs. YOLOX still requires NMS and transpose operations which are unsupported on the DLA, representing <1% of all layers. The small and medium parameterizations are used with input sizes 320, 480 and 480, 640 respectively. The standalone performances of all YOLOv10 and YOLOX models we use are given in Appendix A.4. Furthermore, we use RF-DETR with *nano*, *small*, and *medium* parameterizations all with input sizes 160, 320 480, and 640. Latency limitations prevent using an input size above 640. RF-DETR is used in Section 5.3 alongside the YOLOX models to demonstrate the versatility of *DRIFT* across various OD model architectures.

The chosen input size and parameter count pairs represent a distribution of latencies allowing a range of latency/accuracy tradeoffs to be targeted with DLA based schedules. The DLA models are quantized to integer-8 precision using the COCO17 validation images because the DLA is optimized for integer-8 computation only. For tracking, we utilized ByteTrack, which is an industry standard tracking solution which does not require additional DNN inferences to produce good tracking results.

Datasets: We use the MOT17 dataset to evaluate our methodology. This data set was chosen because it contains a variety of scenarios that encapsulate driving, navigating through pedestrians, and static camera setups. It also has a high variation in the density, size, and location of objects that must be detected and tracked.

Evaluation setup: We establish the baseline to use a single YOLOv10 medium model for object detection with an input size of 1280x1280. This configuration achieves the maximum possible accuracy under 30ms *end-to-end latency*, which includes data transfer, pre-processing, inference, and post-processing of the output data. Post-processing accounts for less than 1% of end-to-end latency, and it is the same across all DNNs. To allow for larger image sizes on the Orin, we implement a custom CUDA kernel to pre-process the frames, avoiding any CPU bottlenecks. *The ground-*

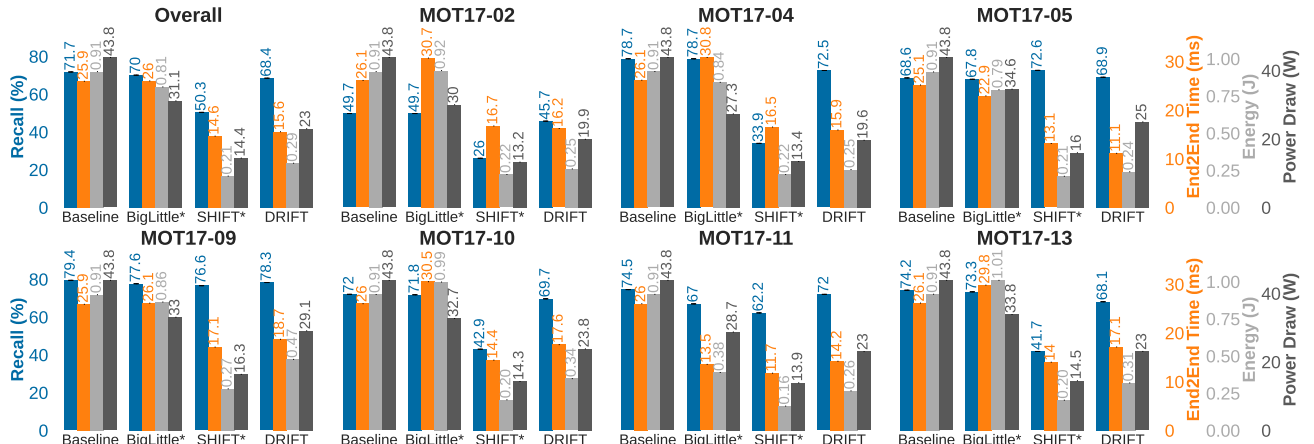


Figure 9: Comparison of baseline YOLOv10, SHIFT and BigLittle with *DRIFT*. The low priority accuracy knob was set to 0.5 for all scenarios and the priority detection classes used were people and vehicles with recall computed using those class labels. Recall (blue) is bigger-is-better, while end2end latency (orange), energy (light gray), and power draw (dark gray) are smaller-is-better metrics.

truth high priority regions are the regions determined from the detection output of the baseline model. The accuracy, reported as the recall, is computed based on the annotations provided by MOT17.

Comparisons: We compare *DRIFT* with the baseline model (*i.e.*, single YOLOv10), and our adaptations of BigLittle (Park et al., 2015) and SHIFT (Davis & Belviranli, 2024). We select these two studies because they both aim to achieve energy-efficient object detection on compute-limited systems, hence they are the closest state-of-the-art approaches whose implementations are available.

BigLittle is adapted from the initial classification task, by using the mean confidence score for a given image to act as the differentiating factor. The confidence threshold to determine when to use the larger model is found using the COCO17 validation dataset. The two DNNs we use for this approach are the baseline YOLOv10 medium model with 1280x1280 input size and YOLOv10 nano with 640x640. *SHIFT* is adapted from the single-class single-object method, considering the aggregate confidence values when constructing their accuracy estimation method. As such, for any given frame, instead of using the top confidence score of the desired class, the mean confidence score of all detections is utilized. COCO17 validation data is again used to generate the offline characteristics required for its runtime. Since both implementations require modification, we will label them as BigLittle* and SHIFT* in the results.

5 RESULTS

The primary results on the MOT17 dataset are shown in Figure 9. We report accuracy (*i.e.*, *Recall*), latency (*i.e.*, *End2End Time*), total *Energy* spent and average *Power Draw* for each MOT17-* scenario individually and also present an *Overall* corresponding to the mean of the values in all scenarios. The reported end-to-end latencies include all overheads such as scheduling and preprocessing. Recall

corresponds to the portion of ground truth objects detected, important for understanding the capability of each method.

5.1 Scenes with Single-class HP Objects

MOT17-02 and **MOT17-09** are static camera scenarios in which people are moving across a pedestrian area and there are no vehicles. In **MOT17-02**, people are mainly small and occupy a horizontal strip of the scene. SHIFT conserves computational resources, but suffers a severe degradation in recall. BigLittle spends more resources, since the single confidence score threshold is consistently below the value deemed acceptable for shortcut detection. *DRIFT* is able to opportunistically schedule detection models which use fewer resources and achieve the same accuracy by focusing on a smaller subset of each frame. In particular, *DRIFT* uses more energy and power consumption within the same latency envelope, showcasing how the utilization of additional inferences and parallel hardware is key to improving accuracy. In **MOT17-09**, the primary challenge is to recover detection on the entire scene once the HP region is smaller. SHIFT is capable of maintaining detection recall while achieving speedup compared to baseline. BigLittle sees a slight degradation in accuracy and latency since it spends extra resources running a small inference for every frame. *DRIFT* is able to achieve baseline accuracy while saving latency / energy / power consumption, but not as significantly as other scenes. This is because there are few exploitable subsequences where HP and LP splits are consistent.

MOT17-11 is a scenario with a moving camera with people occupying a wide variety of areas inside of a shopping mall. The HP region changes frequently, meaning that LP detection must adequately find objects moving in the scene. In this scenario, we observe that BigLittle is able to make gains in all metrics due to a clear correlation in confidence score and accuracy. In particular, SHIFT makes similar improvements in overall performance since it also changes behavior based on runtime confidence scores. *DRIFT*

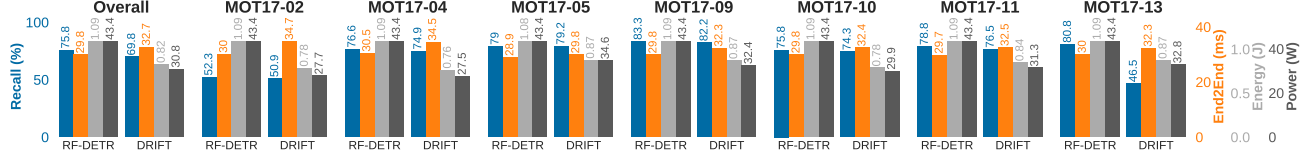


Figure 10: Comparision of baseline RF-DETR model and DRIFT using RF-DETR (GPU) + YOLOX (DLA).

maintains the accuracy while achieving savings relative to the baseline model.

5.2 Scenes with Multi-class HP Objects

MOT17-04 is filmed using a static elevated camera on a busy street where two classes of objects, *i.e.*, *person* and *vehicle*. The frames are close to fully occupied by high-priority detection classes, meaning there exists little room for optimizing detection without sacrificing accuracy. Notably, BigLittle requires the use of two DNNs when confidence is low, resulting in a high end-to-end latency. SHIFT attempts to perform too much optimization on the object detection model latency, resulting in severe accuracy degradation. We observe that *DRIFT* has some accuracy loss, but with a decrease in overall processing latency primarily due to the input size scaling heuristic.

MOT17-05 is shot by a camera moving through people on the street. In the beginning of the scene, there are pedestrians and vehicles moving along the roadway. The majority of early frames have the high-priority bounding region taking up the entire frame, but for only a few large objects making the scenario easy to detect. Large and easy-to-detect objects result in SHIFT being able to make a significant improvement in runtime latency. However, despite BigLittle also using confidence score values to look for performance gains, the simple threshold method cannot make significant improvements. Meanwhile, *DRIFT* was able to make significant improvements, as there were either consistent LP regions that could be exploited, or the input size scaling heuristic allowed more efficient computation.

MOT17-10 and **MOT17-13** are scenarios in which the camera moves through a less crowded street. In **MOT17-10**, there are few pedestrians, which occupy a small region, and vehicles to the opposite side in the early frames. **MOT17-13** is the hardest, since the objects vary in position and size along a thin horizon, and the scene itself changes significantly from start to end. Both BigLittle and SHIFT face challenges in achieving performance gains. This is either due to the necessity of running both models –since the small model’s substantial inferiority limits its usefulness– or because the confidence values fail to align effectively with the complexity of the detection task. *DRIFT* is able to maintain 97% the accuracy of the baseline, while achieving a speedup of 1.48x since it does not rely on confidence values as the only method with identified optimization potential.

Overall: BigLittle improves latency, energy, and power draw in two of the seven sequences, while maintaining

accuracy within 90% of the baseline in 7/7. BigLittle fails because it optimizes for the best computation time when the detection task is easy, but when the detection task is difficult or changes, it results in a runtime worse than the baseline model it utilizes. SHIFT improves latency, energy, and power draw in all sequences, but only achieves the accuracy margin of 90% in 2/7 sequences. SHIFT fails because it aggressively attempts to optimize performance together with accuracy by altering model parameter size, input size, and accelerator target based only on the mean output confidence score. This results in poor detection accuracy, since a model can produce high-confidence results when only detecting a few objects. ***DRIFT* achieves an improvement in all performance metrics and achieves accuracy comparable to baseline in all scenarios**, by considering the detection task as a parallelization problem within MOT and allocating faster computational resources for high priority objects in the scene.

5.3 DETR

To demonstrate that *DRIFT* could flexibly operate with different types of OD models, we replace the DNN-based model that we use for HP regions with transformer-based RF-DETR (Robinson et al., 2025) variations and compare with whole frame RF-DETR baselines. The results are presented in Figure 10. We observe that *DRIFT* saves overall energy cost by utilizing smaller parameterizations of RF-DETR alongside DLA inference at runtime. However, *DRIFT* has an increased latency cost compared to RF-DETR. This latency increase is the result of multiple factors relating to the RF-DETR architecture. Firstly, RF-DETR does not gain significant speedup when lowering parameter size. Second, the limited input size range restricts scheduling capabilities. Third, the combination of model detections becomes significant since RF-DETR produces more detections, resulting in slowdown during NMS. Overall, *DRIFT* showcases adaptability across a wide-variety of model architectures.

5.4 MOT Metrics and Validation

To validate whether the detection accuracies achieved by *DRIFT* translate into tracking accuracy, we evaluate the

Metric	0.4	0.5	0.6	0.7	0.8	0.9
Time (ms)	15.2	15.6	16.8	17.8	19.3	20.3
Energy (J)	0.29	0.30	0.36	0.41	0.48	0.54
Powerdraw (W)	23.3	23.0	24.9	26.4	28.4	29.8
DLA Usage	66.3%	33.5%	13.4%	9.5%	7.5%	5.5%
Baseline Usage	2.8%	2.8%	13.6%	23.9%	41.5%	53.7%

Table 2: Varying LP accuracy goal values and the effect on runtime metrics and schedules.

Schedule	17-02	17-04	17-05	17-09	17-10	17-11	17-13
Baseline	0.17%	0.10%	0.12%	20.9%	0.15%	3.67%	0.13%
GPU+GPU	63.3%	74.4%	72.0%	45.1%	62.8%	58.4%	60.1%
GPU+DLA	36.5%	25.5%	27.8%	33.9%	37.0%	37.9%	39.7%

Table 3: Scheduling decision distribution across GPU+GPU, GPU+DLA executions, and baseline single model fallback on each MOT17 scenario.

YOLOv10 baseline, BigLittle, SHIFT and *DRIFT* using MOT17 ground truths for pedestrian tracking. All methods use ByteTrack as the tracking algorithm with default configurations from the authors' original implementations to ensure fairness. The results presented in Table 4, show that *DRIFT*, with the high-priority class set to people, achieves **99.7%** of the baseline detection accuracy while providing a **1.66x** speed-up in the overall data set. Furthermore, *DRIFT*, outperforms the baseline in all tracking metrics (HOTA, MOTA, IDF1). Of the mean latency reported in Table 4, 85.1% (13.34ms) is attributed to frame pre-processing and OD model inference, while total overhead, including scheduling and image stitching, accounts for 14.9% (2.32ms) per frame, with 1.29ms being spent on framepacking and 1.03ms being spent on scheduling on average.

Figure 11 presents the range of energy consumption and latency across the frames in each sequence while Table 3 shows the distribution of schedules utilized. On sequences with less optimization potential, such as MOT17-09, *DRIFT* often falls back to the baseline. In contrast, for heavily optimizable sequences like MOT17-13, baseline usage is minimal, with the highest DLA-based schedules. Depending on the position and density of objects, *DRIFT* is able to produce a range of schedules that optimize the accuracy-latency-energy trade-off.

5.5 LP Accuracy Goal Knob

To ensure that the estimation methodology has the intended effect on the accuracy performance of the system, we evaluate *DRIFT* using multiple settings for the low-priority accuracy knob, which is provided to our scheduler given

Methodology	DetA (%)	HOTA (%)	MOTA (%)	IDF1 (%)	Latency (ms)
YOLOv10 M 1280x1280	41.82	11.64	6.45	9.21	25.91
YOLOv10 S 1280x1280	39.69	11.81	7.80	9.16	16.66
YOLOv10 N 1280x1280	37.35	11.40	7.89	9.97	12.22
BigLittle*	41.46	11.52	7.06	9.05	25.99
SHIFT*	19.01	11.11	8.44	9.49	14.64
<i>DRIFT</i> People	41.70	11.78	7.76	9.28	15.65

Table 4: Metrics calculated against the pedestrian class on the MOT17 dataset. Evaluation is conducted using the official MOT17 evaluation software (Jonathon Luitjen, 2020). DetA is the detection accuracy, HOTA is higher order tracking accuracy, MOTA is multi-object tracking accuracy, and IDF1 is identity F1 score.

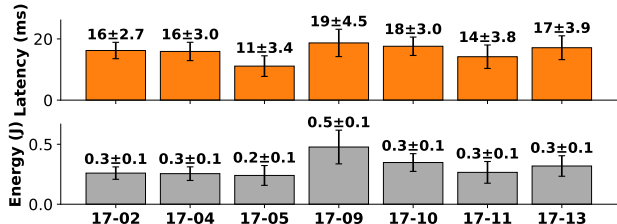


Figure 11: Range in latency and energy usage during runtime of *DRIFT* on each sequence in the MOT17 dataset.

in Algorithm 1 with the *LP accuracy goal* parameter, γ_{lp} . The results of this sensitivity analysis are presented in Table 2. As expected, when the LP knob is increased, more compute-intensive DNNs are scheduled. The nonlinear relationship on power draw is due to whether DLA-based schedules are used or not. If the LP knob is set to lower than or equal to 0.5, GPU-DLA schedules become more balanced. If the knob is set higher, the precision limitations of the DLA-based models do not meet the desired accuracy, hence resulting in schedules that do not use DLA.

5.6 Stability Analysis

To assess whether the stochastic nature of simulated annealing has a significant effect on the average performance of runtime, a stability analysis was performed in which *DRIFT* was run ten times for each sequence in the MOT17 dataset with a unique random seed. The standard deviations are as follows: recall: 0.06%, precision: 0.01%, f1: 0.06%, latency 0.13 ms, energy: 0.005 J and power draw: 0.23 W. Analyzing the produced schedules, there is a 0.4% standard deviation in the amount of GPU-GPU vs. GPU-DLA sub-schedules utilized. **The low variation in run-to-run accuracy and performance metrics demonstrates that *DRIFT* consistently provides the desired accuracy for HP objects while producing precise computational schedules that meet the constraints.**

5.7 Ablation Study

We provide an ablation study in Appendix A.3.

6 CONCLUSION

We introduce *DRIFT* to address the challenge of improving the efficiency of multi-object tracking (MOT) on heterogeneous system-on-chips (SoCs). By grouping objects based on assigned priority classes, *DRIFT* optimizes the use of multiple accelerators to enhance latency and energy consumption without compromising accuracy. Through the use of two separate contextual regions based on object priority, *DRIFT* can allocate computation dynamically reducing latency and saving energy. The effectiveness of *DRIFT* is demonstrated on the MOT17 dataset where it achieves a reduction of up to 2.2x in latency, 3.8x in energy, and 2.2x in power draw while maintaining 99.7% of detection accuracy of high-priority detections.

550 REFERENCES

- 551 Chen, J., Huang, H.-W., Rupp, P., Sinha, A., Ehmke, C.,
552 and Traverso, G. Closed-loop region of interest enabling
553 high spatial and temporal resolutions in object detection
554 and tracking via wireless camera. *IEEE Access*, 9:87340–
555 87350, 2021.
- 556 Dagli, I. and Belviranli, M. E. Shared memory-contention-
557 aware concurrent dnn execution for diversely heteroge-
558 neous system-on-chips. In *ACM SIGPLAN Symposium on*
559 *Principles and Practice of Parallel Programming (PPoPP*
560 *'24)*, 2024.
- 561 Dagli, I., Cieslewicz, A., McClurg, J., and Belviranli, M. E.
562 Axonn: Energy-aware execution of neural network infer-
563 ence on multi-accelerator heterogeneous socs. In *DAC*,
564 pp. 1069–1074, 2022.
- 565 Davis, J. and Belviranli, M. E. Context-aware multi-model
566 object detection for diversely heterogeneous compute
567 systems. In *DATE*, pp. 1–6. IEEE, 2024.
- 568 Dhonde, A., Guntur, P., and Palani, V. Adaptive roi with
569 pretrained models for automated retail checkout. In *CVPR*
570 *Workshops*, pp. 5507–5510, June 2023.
- 571 Du, Y., Zhao, Z., Song, Y., Zhao, Y., Su, F., Gong, T., and
572 Meng, H. Strongsort: Make deepsort great again. *IEEE*
573 *Transactions on Multimedia*, 25:8725–8737, 2023.
- 574 Fang, B., Zeng, X., and Zhang, M. Nestdnn: Resource-
575 aware multi-tenant on-device deep learning for continu-
576 ous mobile vision. In *MobiCom*, pp. 115–127, 2018.
- 577 Ge, Z., Liu, S., Wang, F., Li, Z., and Sun, J. Yolox: Exceed-
578 ing yolo series in 2021. *arXiv preprint arXiv:2107.08430*,
579 2021.
- 580 Girshick, R. Fast r-cnn, 2015. URL <https://arxiv.org/abs/1504.08083>.
- 581 Girshick, R., Donahue, J., Darrell, T., and Malik, J. Rich
582 feature hierarchies for accurate object detection and se-
583 mantic segmentation, 2014. URL <https://arxiv.org/abs/1311.2524>.
- 584 Gokarn, I., Sabbella, H., Hu, Y., Abdelzaher, T., and
585 Misra, A. Mosaic: Spatially-multiplexed edge ai
586 optimization over multiple concurrent video sensing
587 streams. In *Proceedings of the 14th ACM Multi-
588 media Systems Conference, MMSys '23*, pp. 278–288,
589 New York, NY, USA, 2023. Association for Comput-
590 ing Machinery. ISBN 9798400701481. doi: 10.1145/
591 3587819.3590986. URL <https://doi.org/10.1145/3587819.3590986>.
- 592 Jiang, S., Lin, Z., Li, Y., Shu, Y., and Liu, Y. Flexible high-
593 resolution object detection on edge devices with tunable
594 latency. In *Proceedings of the 27th Annual International*
595 *Conference on Mobile Computing and Networking, Mobi-
596 Com '21*, pp. 559–572, New York, NY, USA, 2021. Asso-
597 ciation for Computing Machinery. ISBN 9781450383424.
598 doi: 10.1145/3447993.3483274. URL <https://doi.org/10.1145/3447993.3483274>.
- 599 Jonathon Luiten, A. H. Trackeval. <https://github.com/JonathonLuiten/TrackEval>, 2020.
- 600 Korte, B. and Vygen, J. *Combinatorial Optimization: Theory and Algorithms*. Algorithms and Com-
601 binatorics. Springer Berlin Heidelberg, 2007. ISBN
602 9783540718444. URL <https://books.google.com/books?id=UnYwgPltSjwC>.
- 603 Lee, R., Venieris, S. I., and Lane, N. D. Deep neu-
604 ral network-based enhancement for image and video
605 streaming systems: A survey and future directions.
606 *ACM Comput. Surv.*, October 2021. ISSN 0360-0300.
607 doi: 10.1145/3469094. URL <https://doi.org/10.1145/3469094>.
- 608 Liang, C., Zhang, Z., Zhou, X., Li, B., Zhu, S., and Hu,
609 W. Rethinking the competition between detection and
610 reid in multiobject tracking. *IEEE Transactions on Image
611 Processing*, 31:3182–3196, 2022.
- 612 Lin, T.-Y., Maire, M., Belongie, S., Bourdev, L., Girshick,
613 R., Hays, J., Perona, P., Ramanan, D., Zitnick, C. L., and
614 Dollár, P. Microsoft coco: Common objects in context,
615 2015.
- 616 Milan, A., Leal-Taixé, L., Reid, I., Roth, S., and Schindler,
617 K. MOT16: A benchmark for multi-object track-
618 ing. *arXiv:1603.00831 [cs]*, March 2016. URL
619 <http://arxiv.org/abs/1603.00831>. arXiv:
620 1603.00831.
- 621 Pang, J., Qiu, L., Li, X., Chen, H., Li, Q., Darrell, T., and
622 Yu, F. Quasi-dense similarity learning for multiple object
623 tracking. In *CVPR*, pp. 164–173, 2021.
- 624 Panopoulos, I., Venieris, S., and Venieris, I. Carin:
625 Constraint-aware and responsive inference on heteroge-
626 neous devices for single-and multi-dnn workloads. *TECS*,
627 2024.
- 628 Park, E., Kim, D., Kim, S., Kim, Y.-D., Kim, G., Yoon, S.,
629 and Yoo, S. Big/little deep neural network for ultra low
630 power inference. In *CODES+ISSS*, pp. 124–132, 2015.
631 doi: 10.1109/CODES+ISSS.2015.7331375.
- 632 Rastikerdar, M. M., Huang, J., Fang, S., Guan, H., and
633 Ganesan, D. Cactus: Dynamically switchable context-
634 aware micro-classifiers for efficient iot inference. In

605 *MobiSys*'22, pp. 505–518. Association for Computing
606 Machinery, 2024. ISBN 9798400705816. doi: 10.1145/
607 3643832.3661888.

608 Ravindran, R., Santora, M. J., and Jamali, M. M. Multi-
609 object detection and tracking, based on dnn, for au-
610 tonomous vehicles: A review. *IEEE Sensors Journal*,
611 21(5):5668–5677, 2020.

612 Ren, S., He, K., Girshick, R., and Sun, J. Faster r-cnn:
613 Towards real-time object detection with region proposal
614 networks, 2016. URL <https://arxiv.org/abs/1506.01497>.

615 Robinson, I., Robicheaux, P., Popov, M., Ramanan, D.,
616 and Peri, N. Rf-detr. <https://github.com/roboflow/rf-det>, 2025. SOTA Real-Time Object
617 Detection Model.

618 Smith, K., Gatica-Perez, D., Odobez, J., and Ba, S. Evalu-
619 ating multi-object tracking. In *CVPR workshops*. IEEE,
620 2005.

621 Wang, A., Chen, H., Liu, L., Chen, K., Lin, Z., Han, J., and
622 Ding, G. Yolov10: Real-time end-to-end object detection.
623 *arXiv preprint arXiv:2405.14458*, 2024.

624 Wang, C.-Y. and Liao, H.-Y. M. YOLOv9: Learning what
625 you want to learn using programmable gradient informa-
626 tion. 2024.

627 Wojke, N. and Bewley, A. Deep cosine metric learning
628 for person re-identification. In *WACV*. IEEE, 2018. doi:
629 10.1109/WACV.2018.00087.

630 Wojke, N., Bewley, A., and Paulus, D. Simple online and
631 realtime tracking with a deep association metric. In *ICIP*,
632 pp. 3645–3649. IEEE, 2017. doi: 10.1109/ICIP.2017.
633 8296962.

634 Yang, K., Yi, J., Lee, K., and Lee, Y. Flexpatch: Fast and
635 accurate object detection for on-device high-resolution
636 live video analytics. In *INFOCOM'22*.

637 Zhang, Y., Sun, P., Jiang, Y., Yu, D., Weng, F., Yuan, Z.,
638 Luo, P., Liu, W., and Wang, X. Bytetrack: Multi-object
639 tracking by associating every detection box. In *ECCV'21*.

640

641

642

643

644

645

646

647

648

649

650

651

652

653

654

655

656

657

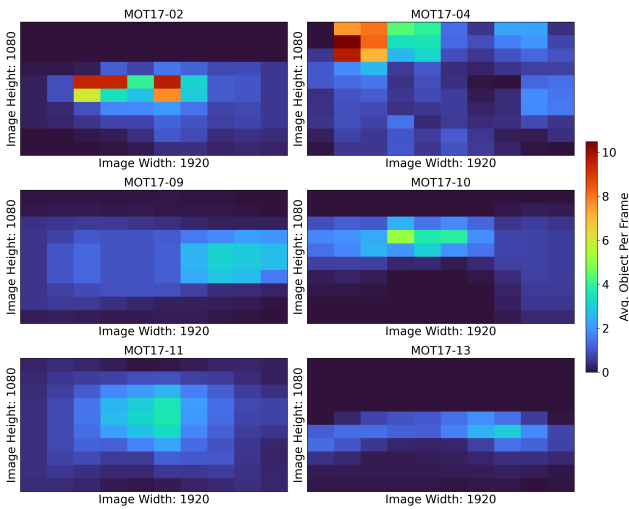
658

659

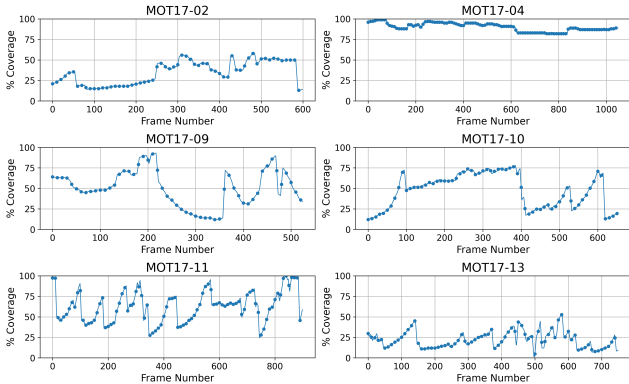
660 A APPENDIX

661 A.1 Object Analysis of MOT Dataset

662 Figure 12 shows a heatmap of the average number of objects
 663 per frame in various MOT sequences. In most scenarios,
 664 there are long sequences of frames with large empty re-
 665 gions which do not contain any objects. Thus, a significant
 666 amount of computational cycles is wasted by processing
 667 these regions. Processing only the relevant data from the
 668 sequence can save latency and energy. Figure 13 expands
 669 on this and shows how the occurrence of objects in real-life
 670 sequences is often cyclic, as objects move in and out of view.
 671 Notably, there are spikes in the amount of coverage when
 672 new objects appear far away from the existing object cluster,
 673 demonstrating the importance of being context-aware and
 674 not focusing only on existing detections. In particular, MOT
 675 scenarios 02, 09, 10, 11, and 13 have significant portions
 676 of the overall sequence where only a subset of a frame is
 677 sufficient to detect all the objects with the same accuracy
 678 that full frame processing would provide. Meanwhile, MOT
 679 scenarios 04 and 05 (the latter is not shown) represent se-
 680 quences in which the spatial information and context of the
 681 objects cannot be used to optimize performance.



693 **Figure 12:** Average number of intersecting objects for each grid-
 694 cell on a frame-by-frame basis for MOT sequences. A 10 by 10
 695 grid a pixel size determined by the frame size is used to compute
 696 the object intersections.



710 **Figure 13:** Percentage of each frame which is occupied by objects.
 711 The object coverage is computed by taking the bounding box of all
 712 object bounding boxes, thus this coverage will be an overestimate
 713 including empty space between objects.

of the overall sequence where only a subset of a frame is sufficient to detect all the objects with the same accuracy that full frame processing would provide. Meanwhile, MOT scenarios 04 and 05 (the latter is not shown) represent sequences in which the spatial information and context of the objects cannot be used to optimize performance.

A.2 Binpacking Algorithm

Algorithm 2 Frame Packing via Shelf Bin Packing

```

Input: Image  $I$ , Groups  $G$ 
Output: Packed Image  $P$ 
1: if  $G = \emptyset$  then
2:   return Empty Image
3: end if
4:  $G \leftarrow \text{sort}(G)$                                  $\triangleright$  Sort descending by size
5:  $ts \leftarrow \text{ceil}(\sqrt{\sum(\text{size}(g) \forall g \in G)})$      $\triangleright$  Target size
6:  $S \leftarrow \emptyset$                                      $\triangleright$  Set of shelves
7: for all  $g \in G$  do
8:   for all  $s \in S$  do
9:     if  $g_{\text{width}} \neq s_{\text{width}} \vee g_{\text{height}} + s_{\text{height}} > ts$  then
10:      continue
11:    end if
12:     $s \leftarrow s \cap \{g\}$ 
13:    break
14:  end for
15:   $S \leftarrow S \cup \{g\}$ 
16: end for
17:  $h \leftarrow \max(s_{\text{height}} \forall s \in S)$ 
18:  $w \leftarrow \sum(s_{\text{width}} \forall s \in S)$ 
19:  $P = \text{image}[h, w]$ 
20:  $frontier \leftarrow 0$ 
21: for all  $s, s_w, s_h \in S$  do
22:   for all  $i \in s_h$  do
23:     for all  $j \in s_w$  do
24:        $\text{bbox} \leftarrow s[i \times s_w + j]_{\text{bbox}}$   $\triangleright$  Get bbox from cell
25:        $\text{bbox}_{\text{new}} \leftarrow \text{getBbox}(i, j)$   $\triangleright$  Get new bbox
26:        $P[\text{bbox}_{\text{new}}] \leftarrow I[\text{bbox}]$   $\triangleright$  Update image
27:     end for
28:   end for
29:    $frontier \leftarrow frontier + s_w$ 
30: end for
31: return  $P$ 
```

A.3 Ablation Study

In order to understand the individual contributions of several optimizations we deploy in *DRIFT*, we conduct an ablation study. We iteratively add features into *DRIFT* and compare the resulting accuracy, latency, and energy usage over the entire dataset. The key features to be assessed are the impact of 1) LP detection and frame packing and 2) the utilization of parallel hardware to augment the performance of the system.

Baseline: The YOLOv10M model with an input size of 1280x1280 representing the standard detection performance.

ROI: A region-of-interest (ROI) strategy that processes only the bounding box of previous HP detections with some padding. If no prior detections exist, the full frame is used. This evaluates accuracy trade-offs from focusing only on relevant regions.

Dynamic: A dynamic model selection approach where we pick a YOLOv10M version with lower resolution input size

715	716	Model Info			Metrics		Input Size							
		717	718	719	720	721	722	723	724	725	726	727	728	729
YOLOv10(Wang et al., 2024)	M	GPU	FP16	Recall	0.4x	0.64x	0.75x	0.83x	0.91x	0.96x	0.99x	1.0x		
				Latency	3.48ms	4.97ms	6.98ms	9.45ms	12.31ms	15.84ms	21.21ms	25.91ms		
				Energy	0.04J	0.07J	0.14J	0.24J	0.37J	0.54J	0.73J	0.91J		
	S	GPU	FP16	Power	17.65W	24.52W	31.29W	35.57W	40.2W	42.0W	43.73W	43.8W		
				Recall	0.36x	0.59x	0.72x	0.8x	0.87x	0.92x	0.96x	0.98x		
				Latency	2.94ms	3.88ms	4.99ms	6.31ms	8.69ms	10.04ms	14.01ms	16.66ms		
	N	GPU	FP16	Energy	0.02J	0.04J	0.07J	0.11J	0.18J	0.25J	0.34J	0.44J		
				Power	15.13W	20.26W	25.27W	29.23W	32.11W	35.51W	36.08W	37.91W		
				Recall	0.28x	0.53x	0.66x	0.75x	0.82x	0.87x	0.92x	0.93x		
YOLOX (Ge et al., 2021)	M	DLA	INT8	Latency	2.82ms	3.63ms	4.35ms	5.02ms	6.68ms	7.51ms	10.59ms	12.22ms		
				Energy	0.02J	0.03J	0.04J	0.06J	0.09J	0.13J	0.18J	0.23J		
				Power	12.72W	13.4W	14.67W	14.79W	14.74W	14.69W	14.75W	15.24W		
	S	DLA	INT8	Recall	0.54x	0.97x	0.99x	1.0x	0.95x	0.96x	0.86x	0.82x		
				Latency	3.18ms	4.51ms	7.08ms	11.21ms	16.42ms	22.87ms	30.46ms	40.05ms		

Table 5: Performance comparision of YOLOv10 and YOLOX models across all MOT17 sequence. All metrics are reported as the average across all sequences on a frame-by-frame basis. Power draw is reported as the total system draw to run the model. Recall is reported relatively on a model-by-model basis.

that matches the ROI bounding box. This approach improves the ROI method and represents the lower bound on latency, energy and power needed to process the HP region using the baseline model (*i.e.*, YOLOv10M).

DRIFT-GPU: This version is based on *DRIFT*'s HP/LP-based MOT execution strategy, but the scheduler only uses GPU and not the DLA. It also considers the impact of LP detection on accuracy and uses the same scheduling mechanism as *DRIFT* but switches back to the baseline model unless HP/LP-based processing is expected to be faster.

DRIFT: The full *DRIFT* system, incorporating GPU-DLA scheduling for optimal performance.

Each method is evaluated on MOT17 as detailed in Section 4. Figure 14 presents the relative speedup of each version for different metrics, in comparison to the previous version.

ROI strategy provides minimal benefits in latency, energy and power draw at the expense of reduced recall. Accuracy loss occurs when detections fall outside the selected region, leading to rapid over-focusing. Latency gains come primarily from reduced data transfer between CPU and GPU before preprocessing.

Dynamically selecting the model with smaller input size based on the ROI size improves performance, but further reduces recall. Moving objects or cameras can cause excessive focusing, and hence omitting important information. While dynamic scaling achieves nearly 1.25x speedup over the baseline, its accuracy-latency trade-off remains inefficient, with significant accuracy losses in highly dynamic scenarios. In contrast, *DRIFT* provides a 1.6x speedup with greater than 3.0x gains in energy usage while maintaining nearly all recall.

DRIFT-GPU showcases the benefits of *DRIFT*'s novel LP

identification and binpacking algorithms with the exception that it does not take advantage of multiple accelerators (*i.e.*, DLAs in addition to GPUs). Therefore, the resulting schedules serialize HP and LP processing on the same GPU. *OnlyGPU* improves accuracy over *ROI* and *Dynamic* methods, while also improving latency, energy, and power draw since it can exploit smaller models for LP regions.

DRIFT, using additional hardware, improves latency more than the *GPU-only* schedules and thus maximizes gains in latency and energy usage (Figure 14). However, compared to GPU-only schedules, the power draw is slightly higher since both accelerators are being used at once. Multi-accelerator execution further optimizes performance, underscoring the importance of LP region processing and full hardware utilization.

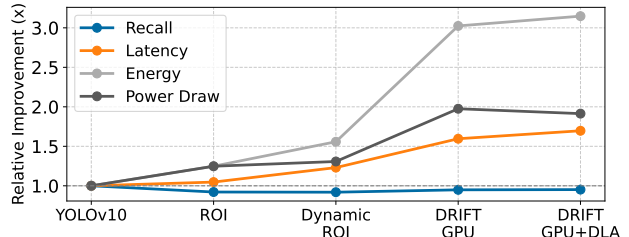


Figure 14: Comparison of various simple methods and portions of the *DRIFT* methodology to identify the important contributions. Evaluated on the MOT17 dataset with results averaged across all video sequences.

A.4 YOLO Model Runtimes

An overview of all YOLOv10 and YOLOX models we use is presented in Table 5.